

Article

Simulating the Effects of the Airborne Lidar Scanning Angle, Flying Altitude, and Pulse Density for Forest Foliage Profile Retrieval

Haiming Qin ^{1,2}, Cheng Wang ^{1,*}, Xiaohuan Xi ¹ , Jianlin Tian ³ and Guoqing Zhou ⁴

¹ Key Laboratory of Digital Earth Science, Institute of Remote Sensing and Digital Earth, Chinese Academy of Sciences, Beijing 100094, China; qinhm@radi.ac.cn (H.Q.); xixh@radi.ac.cn (X.X.)

² University of Chinese Academy of Sciences, Beijing 100049, China

³ School of Civil Engineer and Architecture, Jishou University, Jishou 427099, China; Tian.jianlin@hotmail.com

⁴ Guilin University of Technology, Guilin 541004, China; gzhou@glut.edu.cn

* Correspondence: wangcheng@radi.ac.cn; Tel.: +86-10-8217-8129; Fax: +86-10-8217-8177

Received: 20 April 2017; Accepted: 4 July 2017; Published: 10 July 2017

Abstract: Foliage profile is a key biophysical parameter for forests. Airborne Light Detection and Ranging is an effective tool for vegetation parameter retrieval. Data acquisition conditions influence the estimation of biophysical parameters. To acquire accurate foliage profiles at the lowest cost, we used simulations to explore the effects of data acquisition conditions on forest foliage profile retrieval. First, a 3-D forest scene and the airborne small-footprint full-waveform LiDAR data were simulated by the DART model. Second, the foliage profile was estimated from LiDAR data based on a Geometric Optical and Radiative Transfer model. Lastly, the effects of the airborne LiDAR scanning angle, flying altitude, and pulse density on foliage profile retrieval were explored. The results indicated that the scanning angle was an important factor in the foliage profile retrieval, and the optimal scanning angle was 20°. The optimal scanning angle was independent of flying altitude and pulse density, and combinations of multiple scanning angles could improve the accuracy of the foliage profile estimation. The flying altitude and pulse density had little influence on foliage profile retrieval at plot level and could be ignored. In general, our study provides reliable information for selecting the optimal instrument operational parameters to acquire more accurate foliage profiles and minimize data acquisition costs.

Keywords: airborne full-waveform LiDAR; forest foliage profile; scanning angle; flying altitude; pulse density

1. Introduction

The forest leaf area index (*LAI*), the total one-sided leaf area per unit ground surface area [1], is an important biophysical parameter in ecosystem models [2]. The vertical distribution of the forest leaf area can influence the photosynthesis and carbon stock of the forest [3], and it is often represented by the foliage profile. The foliage profile plays an important role in energy exchange, the water cycle, and the carbon cycle in an ecosystem [4]. As a vertical structure parameter of the canopy, the foliage profile can estimate the forest aboveground biomass [5,6] and net primary productivity (NPP) [7], and it has great potential to describe the distribution of light transmission in the canopy [4]. The foliage profile is also a key factor in determining biodiversity and habitat suitability [8], as different wildlife species live at different forest heights.

Traditional direct foliage profile measurement methods, such as stratified sampling, and indirect ground measurement methods, such as the point-quadrat sampling [9,10], are expensive, labour-intensive, and time-consuming. Moreover, these direct methods are destructive. These

methods cannot be implemented over large areas, and they cannot be used to monitor the vegetation growth conditions over a long time series. Optical remote sensing has been widely used to retrieve vegetation biophysical and biochemical parameters, such as *LAI* [11,12] and chlorophyll content [13,14]. Optical remote sensing can provide information on the horizontal distribution of forest parameters over large areas, but it has difficulty in acquiring the vertical structure of the forest canopy [15,16].

As an active remote sensing technique, light detection and ranging (LiDAR) has a strong penetration ability in the forest canopy, and it can acquire the information from the lower canopy [17]. Full-waveform LiDAR records all backscatter energy; thus, it can capture richer vertical canopy structure information [16]. LiDAR has been used to retrieve many forest structure parameters, such as tree height [18], *LAI* [19,20], and biomass [21]. The forest foliage profile has also been retrieved by LiDAR in recent studies [22,23]. Tang et al. [24] estimated the cumulative *LAI* profile in tropical rain forests based on the Geometric Optical and Radiative Transfer (GORT) model with airborne large-footprint full-waveform LiDAR data, and the results indicated that the estimation moderately agreed with the tower-measured vertical *LAI* profile. Ma et al. [25] retrieved the foliage area volume density (FAVD) profile of a forest using a radiative transfer (RT) model and airborne small-footprint full-waveform LiDAR data. The study then obtained the forest *LAI* which were highly correlated. Zhao et al. [26] compared the conifer stand foliage profiles derived from the terrestrial full-waveform LiDAR (EVI) and airborne full-waveform LiDAR (LVIS) system. The results showed that airborne LiDAR could acquire more upper canopy information and terrestrial LiDAR could capture more information about the lower canopy, and the two methods exhibited strong agreement.

It is believed that data acquisition conditions, such as the scanning angle and flying altitude, could affect the accuracy of vegetation parameter estimations and determine the cost of data acquisition. Several studies have analysed the sensitivity of some vegetation structure parameters to LiDAR data acquisition conditions. Morsdorf et al. [27] analysed the effects of the airborne LiDAR flying height and scanning angle on tree height, fractional cover, and *LAI* estimations. The results indicated that the underestimation of the forest height increased and the fractional cover decreased with the increase in flying altitude. The effect of the scanning angle was not as evident, probably due to the small scanning angle used, but the fractional cover seemed to be most affected by the scanning angle [27]. Lovell et al. [28] simulated airborne LiDAR data to explore the optimal LiDAR data acquisition conditions to estimate forest height. The results showed that the estimated predominant height was affected by the LiDAR sampling interval, and they were linearly dependent. Keränen et al. [29] studied the influences of the scanning angle, flying height, and scanning mode on the inventory of forest parameters. The study found that the flying altitude had little influence on the estimation of plot volume and mean height. The LiDAR data with a scanning angle of 15° could obtain slightly more precise mean height and plot volume measurements than the data with a scanning angle of 20°. Holmgren et al. [30] simulated airborne LiDAR data using a ray-tracing method to explore the effects of the scanning angle on mean height and canopy closure estimations. The results indicated that the influence of the scanning angle on height percentiles was greater in the forests with low intervals than with high intervals, and the effect of the scanning angle on canopy closure was greater than the effect on laser height percentiles. Kükenbrink et al. [31] explored the effects of pulse density and flight strip overlap on occluded and unobserved canopy volumes. The results indicated that the forest canopy volume was obviously occluded, even with a high pulse density, and larger flight strip overlap can significantly increase the amount of observed canopy volume due to the added observation angles and increased pulse density. However, to our knowledge, there has not been a study exploring the effects of LiDAR data acquisition conditions on forest foliage profile retrieval.

To obtain a more accurate forest foliage profile at the lowest cost, it is vital to investigate the effects of data acquisition conditions on foliage profile estimations. The overall goal of our study is to explore the effects of the scanning angle, flying altitude, and pulse density on foliage profile retrieval using simulated airborne full-waveform LiDAR data. The specific objectives of our study are to: (1) simulate the 3-D forest scene and airborne small-footprint full-waveform LiDAR data; (2) retrieve the forest

foliage profile from simulated LiDAR data based on the GORT model; and (3) assess the effects of the scanning angle, flying altitude, and pulse density on foliage profile retrieval.

2. Materials

2.1. Creation of the 3-D Forest Scene

To simulate the LiDAR data, the 3-D forest scene should first be created. OnyxTREE (Version 6.0, Onyx Computing, Inc., Cambridge, MA, USA, 2003) is a vegetation modelling software produced by Onyx computing that has been used in several studies for vegetation structure generation, forest management, and vegetation remote sensing [32]. The software has a rich library including the most common vegetation types, and it can precisely describe the 3-D structure of vegetation. According to the field investigation, we generated 80 Tiliacs using the OnyxTREE software with different parameters such as trunk height and crown diameter. Tilia (*Tilia tuan Szyszyl.*) is a deciduous tree that grows mainly in North America, Europe, and Asia. The tree generated from OnyxTREE was composed of many triangular facets, and it was saved in .obj format. A plane on the ground surface that was free from the terrain effect was chosen, and the plane size was set to 60 m \times 60 m. To create a forest scene, we placed all 80 Tiliacs on the ground surface using random tree centre locations. To avoid edge effects, we selected a sub-region of 40 m \times 40 m in the centre of the scene for the sensitivity analysis. The scene is shown in Figure 1. To acquire the simulated foliage profile of the plot, we layered the plot scene at 1 m height intervals and then calculated the leaf area of each layer by summing the areas of all triangular facets in the layer. We calculated the ratio of the leaf area of each layer to the plot area to acquire the simulated foliage profile. The simulated foliage profile is shown in Figure 2, and the simulated LAI was 4.86.

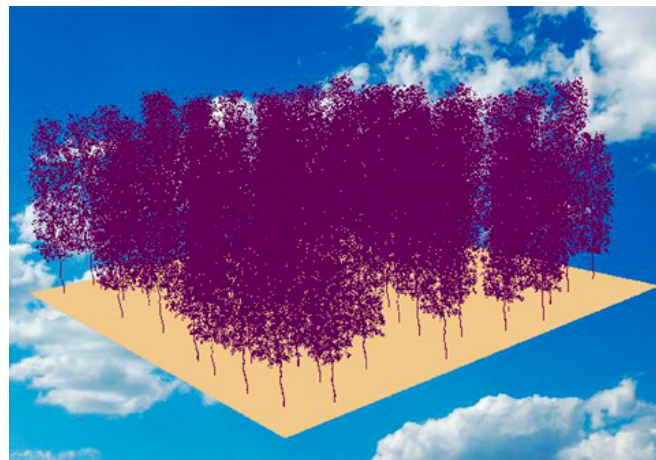


Figure 1. Simulated forest scene.

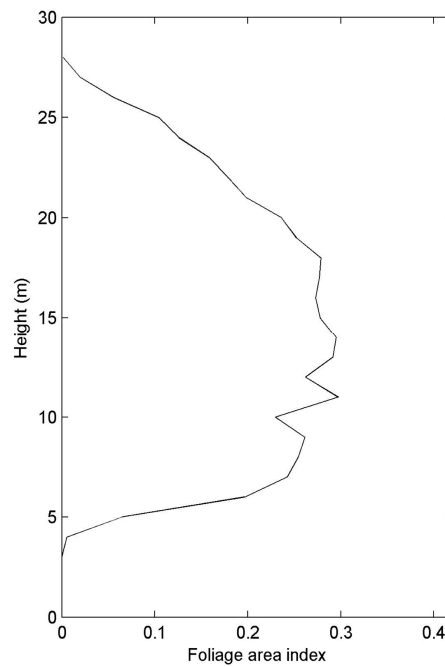


Figure 2. Simulated foliage profile.

2.2. LiDAR Data Simulation

The DART (Discrete Anisotropic Radiative Transfer) model is a comprehensive physics-based 3-D model that can simulate the earth-atmosphere radiation interaction from visible to thermal infrared wavelengths [33–36]. The DART model was developed at Center for the Study of the Biosphere from Space (CESBIO) in 1992 and patented in 2003. We acquired the free DART licenses (DART 5.6.0 V739) from Paul Sabatier University. The model can simulate the optical image and LiDAR data, including both airborne and terrestrial LiDAR data. The simulations even contain discrete return, waveform, and photo counting LiDAR data. We simulated the airborne waveform LiDAR data for the 3-D forest scene created by Onyx TreeMaker using the DART software. To explore the effects of the scanning angle, flying height, and pulse density on forest foliage profile retrieval, we simulated the airborne full-waveform LiDAR data under different conditions using the variable controlling method. The scanning angle was from 0° to 30° at an interval of 5° , the flying height was set from 1000 m to 4000 m with an interval of 1000 m, and the pulse density was set from 0.25 pulse/m² to 8 pulses/m². The beam divergence was set as 0.15 mrad, so the footprint size was set from 0.15 m to 0.6 m with an interval of 0.15 m. The scanning angle is the angle from nadir. The parameters of all simulations are shown in Table 1. The simulated scan schematic is shown in Figure 3, where the green circles represent the trees, the blue arrow represents the flight route and direction, and the vertices of the green grid represent the centres of the footprints. Several examples of simulated single airborne LiDAR pulse data are shown in Figure 4.

Table 1. The airborne LiDAR data acquisition parameters of all simulations.

No.	Scanning Angle (°)	Flying Altitude (m)	Pulse Density (Pulses/m ²)
1	20	2000	0.25
			1
			4
		4000	1
			1
			1
2	20	1000	1
		2000	
		3000	
		4000	
3	20	2000	0.25
			0.5
			1
			2
			4
			8

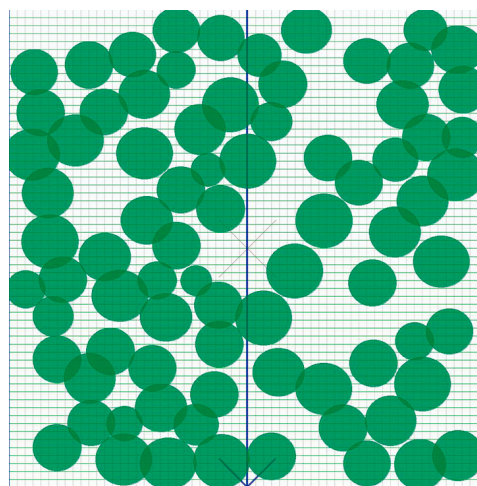


Figure 3. Airborne LiDAR scan schematic (the scanning angle is 0°, and the pulse density is 1 pulse/m²).

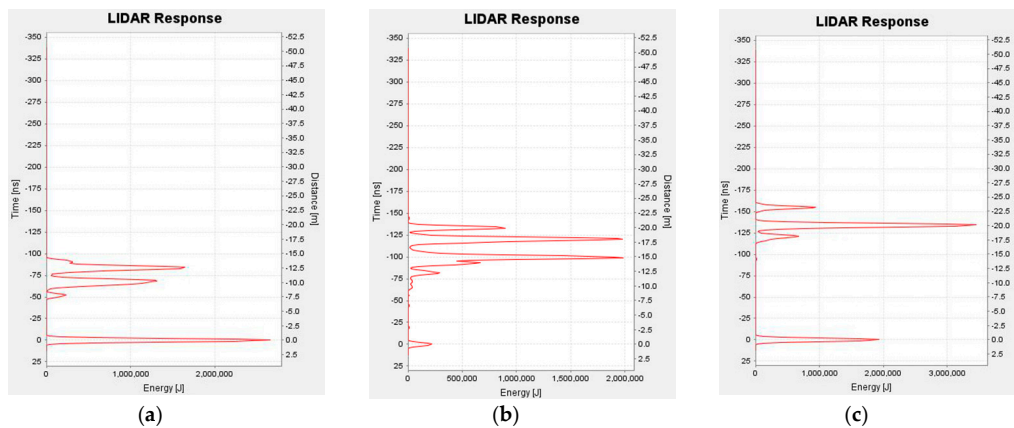


Figure 4. Three examples (a–c) of simulated airborne LiDAR pulse data.

3. Methods

The foliage profile is the vertical distribution of the forest leaf area. The GORT model was used to obtain the foliage profile from the LiDAR data. The raw small-footprint full-waveform LiDAR data were processed using the following steps: waveform stacking, return energy profile generation, cumulative canopy closure profile generation, cumulative leaf area index profile generation, and foliage profile generation [37].

3.1. Waveform Stacking and Return Energy Profile Generation

When the upper vegetation is dense, more energy from a pulse is intercepted by the vegetation, so the small-footprint waveform LiDAR always acquires faint ground return. However, sufficient ground return is important for estimating the vegetation LAI using the method based on the Beer-Lambert law [38]. To enhance the ground returns, the plot size was chosen as the aggregation cell size according to Nie et al. [38], and all small-footprint waveforms within one cell were stacked into a large pseudo-waveform. Using this method, the ground returns could be easily acquired from the pseudo-waveform. After waveform stacking, the return energy profile was generated.

3.2. Canopy Closure Profile Generation

Canopy closure is always calculated as the ratio of canopy return energy to total return energy using Equation (1). Based on the return energy profile, the canopy closure at height z was calculated as the ratio of cumulative canopy return energy from the canopy top to height z to the total return energy, as shown in Equation (2). Then, the canopy closure profile was generated. To eliminate the difference derived from the different reflectance from the ground and the canopy, the reflectance ratio between the vegetation and the ground was considered when calculating the canopy closure profile.

$$f_{\text{cover}} = \frac{E_v}{E_v + E_g}, \quad (1)$$

$$f_{\text{cover}}(z) = \frac{E_v(z)}{E_v(0) + \frac{\rho_v}{\rho_g} E_g}, \quad (2)$$

where f_{cover} represents the canopy cover of the whole canopy; $f_{\text{cover}}(z)$ represents the canopy cover from the canopy top to height z ; E_v and E_g are the whole canopy return energy and ground return energy, respectively; $E_v(z)$ and $E_v(0)$ are the canopy return energies from the canopy top to height z and from the canopy top to height 0, respectively; and ρ_v and ρ_g are the reflectance of the vegetation and the ground, respectively.

3.3. Cumulative Leaf Area Index Profile Generation

Based on the Beer-Lambert law, the cumulative leaf area index profile was retrieved from the cumulative canopy closure profile according to Equation (3).

$$LAI_{\text{cum}}(z) = -\frac{\log(1 - f_{\text{cover}}(z))}{G \times \Omega}, \quad (3)$$

Where $LAI_{\text{cum}}(z)$ is the cumulative leaf area index from the canopy top to height z and G is the projection coefficient. It is assumed that the foliage is distributed randomly, so G is set to 0.5. Ω is the clumping index. According to the global foliage clumping index derived by Chen et al. [39], we chose 0.63 as the value of Ω , which was the mean clumping index for a broadleaf and evergreen forest.

3.4. Foliage Profile Generation

To obtain the vertical distribution of the leaf area index, we calculated the derivative with respect to the cumulative leaf area index according to Equation (4), and the foliage profile was then acquired.

$$f_{\text{foliage_profile}}(z) = \frac{dLAI_{\text{cum}}(z)}{dz}, \quad (4)$$

where $f_{\text{foliage_profile}}(z)$ is the foliage profile at height z .

3.5. Accuracy Assessment

To assess the accuracy of the forest foliage profile estimation, the root mean squared errors (*RMSEs*) of the simulated foliage profile and the retrieved foliage profiles under all data acquisition conditions were calculated according to Equation (5). When the *RMSE* was lower, the estimation accuracy was higher. The absolute difference between the simulated leaf area index and the retrieved total leaf area index (*Diff*) could also be used to assess the foliage profile retrieval accuracy, and the calculation method is shown in Equation (6). The estimation accuracy was higher when the absolute difference was lower.

$$RMSE = \sqrt{\frac{\sum_{i=1}^n (\hat{y}_i - y_i)^2}{n}}, \quad (5)$$

$$Diff = |LAI_{\text{simulated}} - LAI_{\text{retrieved}}|, \quad (6)$$

where \hat{y}_i represents the retrieved foliage profile value in the i th layer, y_i represents the simulated foliage profile value in the i th layer, and n represents the number of layers. The $LAI_{\text{simulated}}$ represents the simulated total *LAI*, $LAI_{\text{retrieved}}$ represents the retrieved total *LAI*, and *Diff* represents the absolute difference between $LAI_{\text{simulated}}$ and $LAI_{\text{retrieved}}$.

4. Results

4.1. Estimation of Foliage Profile

An example of the process used to estimate the forest foliage profile of the plot is shown in Figure 5. The scanning angle, flying altitude, and pulse density in the example were 20°, 2000 m, and 1 pulse/m², respectively. The red line in Figure 5 was the dividing line between the ground and the canopy. Figure 5a shows the return energy profile of the plot. We can see that the height range of the canopy return energy was larger than the height range of the ground return energy, and the canopy return energy varied with the increase in tree height. The canopy closure profile is shown in Figure 5b. Figure 5b indicates that the canopy closure increased as the tree height decreased, and the rate of change was different at different heights. The total canopy closure was 0.74. Figure 5c represents the cumulative *LAI* profile, and it showed that the cumulative *LAI* increased as the tree height decreased. The total *LAI* was 4.94. Therefore, the difference between the simulated total *LAI* and the retrieved total *LAI* was 0.08. Figure 5d represents the forest foliage profile, and it demonstrated that the single-layer foliage area index varied with the increase of tree height. The single-layer foliage area index at the middle heights was larger than at the lower or higher heights, and the largest value was 0.33.

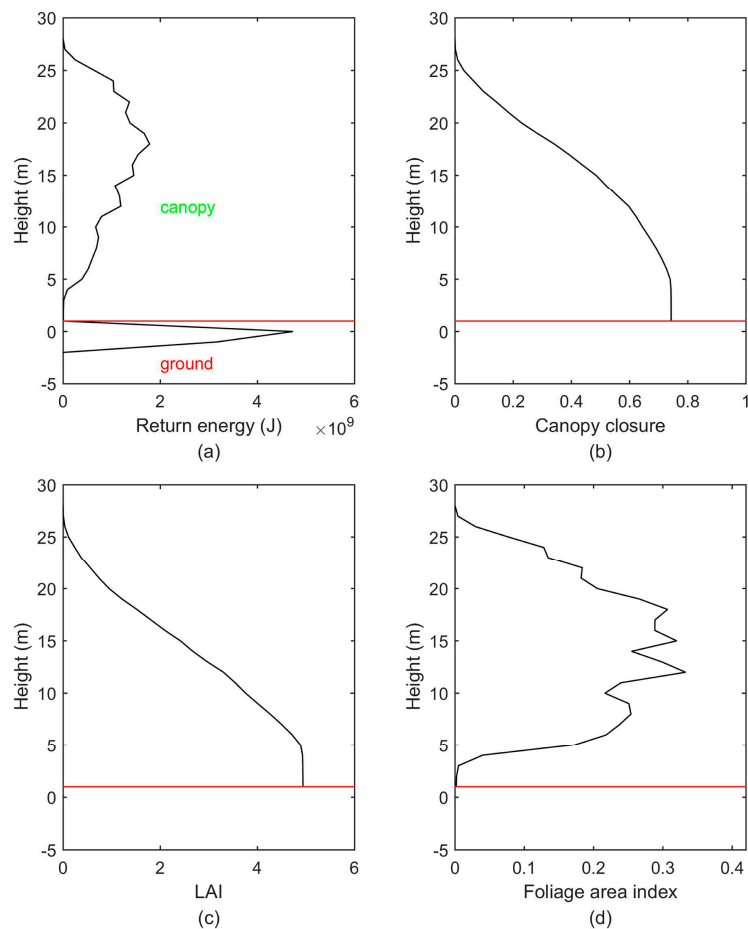


Figure 5. An example of foliage profile processing stages for the plot when the scanning angle, flying altitude, and pulse density are 20° , 2000 m, and one pulse/m², respectively: (a) return energy profile; (b) cumulative canopy closure profile; (c) cumulative LAI profile; (d) foliage profile.

4.2. Effect of Scanning Angle on Foliage Profile Estimation

To investigate the influence of the airborne LiDAR scanning angle on foliage profile retrieval, we estimated the forest foliage profiles from the LiDAR data at scanning angles from 0° to 30° at 5° intervals. The retrieved forest foliage profiles at all scanning angles are shown in Figure 6a, and the histograms of the retrieved foliage profiles at each scanning angle are shown in Figure 6b–h. Figure 6a indicates that when the scanning angle was 0° , the foliage profile was smallest at lower canopy heights and largest at higher canopy heights. When the scanning angle was 30° , the foliage profile was largest at the lower canopy heights and smallest at higher canopy heights. In the lower canopy, which was lower than 18 m, the foliage profile increased with the increase of the scanning angle. However, in the upper canopy, which was higher than 18 m, the foliage profile decreased with the increase of the scanning angle, and the rate of change was low.

The RMSEs of the simulated foliage profiles and the estimated foliage profiles and the *Diff*s of the simulated total LAIs and the retrieved total LAIs at all scanning angles were calculated to quantitatively assess the accuracy of the foliage profile estimation, and the results are shown in Figure 7. Figure 7a demonstrates that the RMSE decreased when the scanning angle increased from 0° to 20° , and it increased when the scanning angle increased from 20° to 30° . Therefore, when the scanning angle was 20° , the estimated foliage profile had the lowest RMSE. Figure 7b showed that the *Diff* decreased when the scanning angle increased from 0° to 20° , and it increased when the scanning angle increased from

20° to 30°. The total LAI estimated at the scanning angle of 20° was the closest to the simulated LAI. Therefore, when the scanning angle was 20°, the estimated foliage profile had the highest accuracy.

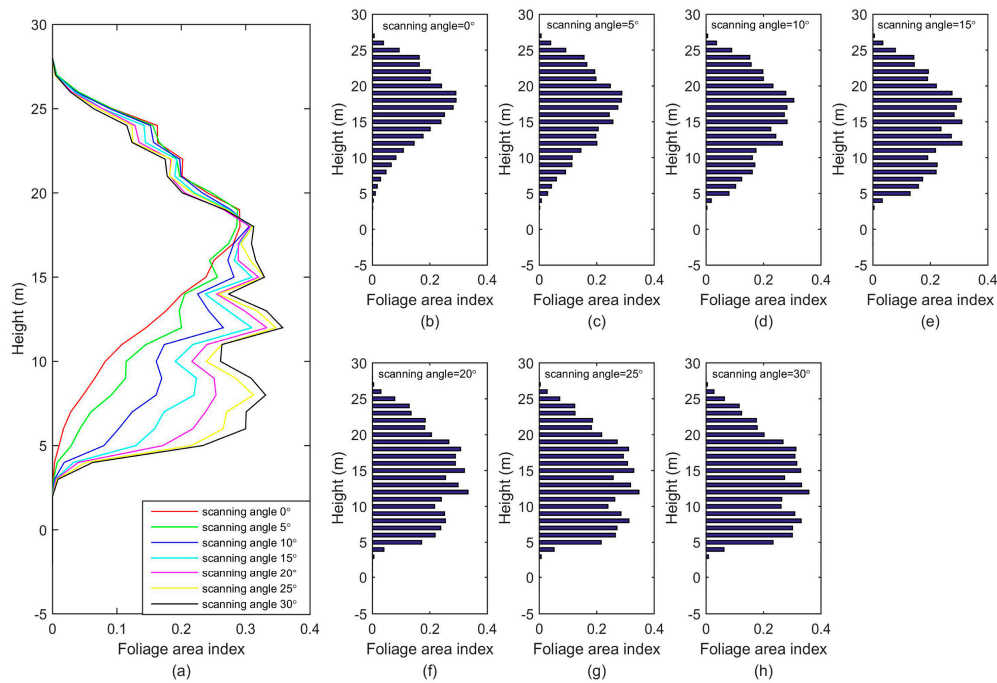


Figure 6. The estimated foliage profiles at the scanning angles from 0° to 30° at 5° intervals (the flying altitude and pulse density are 2000 m and one pulse/m², respectively). (a) The estimated foliage profiles at all scanning angles; (b–h) the histograms of the estimated foliage profiles at the scanning angles of 0°, 5°, 10°, 15°, 20°, 25°, 30°.

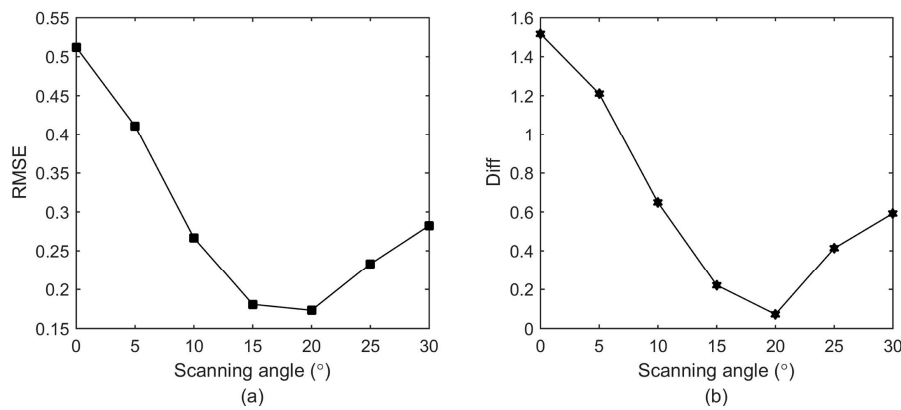


Figure 7. The RMSEs of the foliage profiles (a) and the *Diffs* of the total LAIs (b) at scanning angles from 0° to 30° at 5° intervals (the flying altitude and pulse density are 2000 m and one pulse/m², respectively).

To investigate whether the optimal scanning angle is dependent on the flying altitude, we estimated the forest foliage profiles from the LiDAR data at all scanning angles at flying altitudes of 2000 m and 4000 m. The RMSEs and the *Diffs* are shown in Figures 7 and 8, respectively. Figure 8a,b show that the RMSE and *Diff* both decreased when the scanning angle increased from 0° to 20°, and they increased when the scanning angle increased from 20° to 30°. Therefore, when the forest foliage profile was estimated from the LiDAR data at a flying altitude of 4000 m, the optimal scanning angle was 20°, which was the same as the results at a flying altitude of 2000 m. In conclusion, these results indicated that the optimal scanning angle is unrelated to the flying altitude.

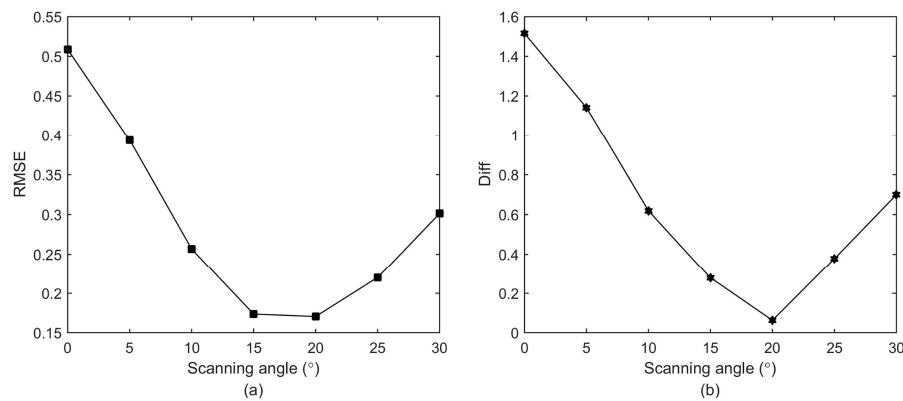


Figure 8. The *RMSEs* of the foliage profiles (a) and the *Diffs* of the total *LAI* (b) at scanning angles from 0° to 30° at 5° intervals (the flying altitude and pulse density are 4000 m and one pulse/m², respectively).

To explore whether the optimal scanning angle is dependent on the pulse density, we estimated the forest foliage profiles from the LiDAR data at all scanning angles at pulse densities of 0.25 pulse/m², one pulse/m², and four pulses/m². The *RMSEs* and *Diffs* were all calculated, and the results are shown in Figure 7, Figure 9, and Figure 10. Figures 9 and 10 show that the *RMSEs* and *Diffs* all first decreased and then increased, and the minimum values were reached at a scanning angle of 20°, which was the same as the results in Figure 7. Therefore, when the pulse density increased from 0.25 pulse/m² to four pulses/m², the optimal scanning angle for foliage profile retrieval at plot level remained at 20°, which demonstrated that the optimal scanning angle was independent of the pulse density at plot level when the pulse density increased from 0.25 pulse/m² to four pulses/m².

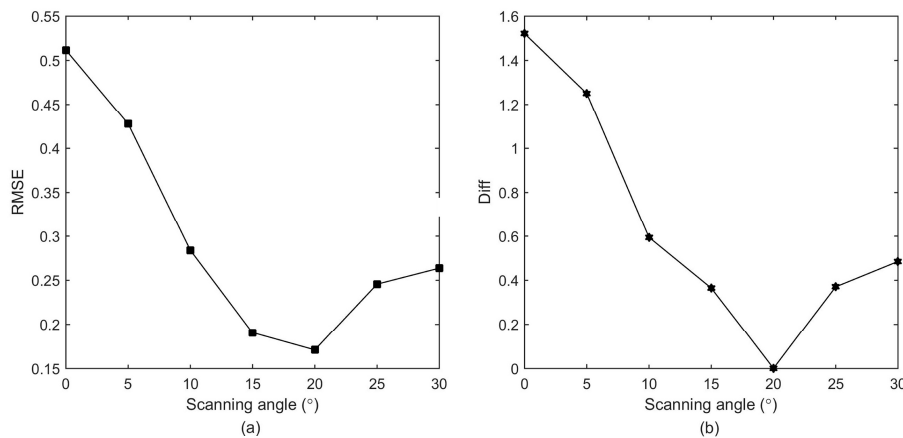


Figure 9. The *RMSEs* of the foliage profiles (a) and the *Diffs* of the total *LAI* (b) at scanning angles from 0° to 30° at 5° intervals (the flying altitude and pulse density are 2000 m and 0.25 pulse/m², respectively).

To determine if combining multiple scanning angles can improve the accuracy of foliage profile estimations, we estimated the foliage profile from the LiDAR data at all single scanning angles and combinations of scanning angles. The *RMSEs* and *Diffs* were calculated to assess the estimation accuracies. Figure 11 shows that when using a single scanning angle, the *RMSE* at the scanning angle of 20° was smallest, and it was 0.17. When using a combination of scanning angles to estimate the foliage profile, the *RMSEs* of the 15° and 20°, 15° and 25°, and 15° and 30° combinations were all smaller than 0.17. When the scanning angles of 15° and 20° were combined, the *RMSE* was the smallest, at 0.16. Figure 12 demonstrates that when using a single scanning angle, the *Diff* at the scanning angle of 20° was 0.072, which was the smallest. When using a combination of scanning angles to estimate the foliage profile, the *Diff* of the 15° and 25° and 15° and 30° combinations were smaller than 0.072.

When the scanning angles of 15° and 25° were combined, the *Diff* was the minimum, and it was 0.013. Therefore, combining multiple scanning angles could improve the accuracy of the forest foliage profile estimation.

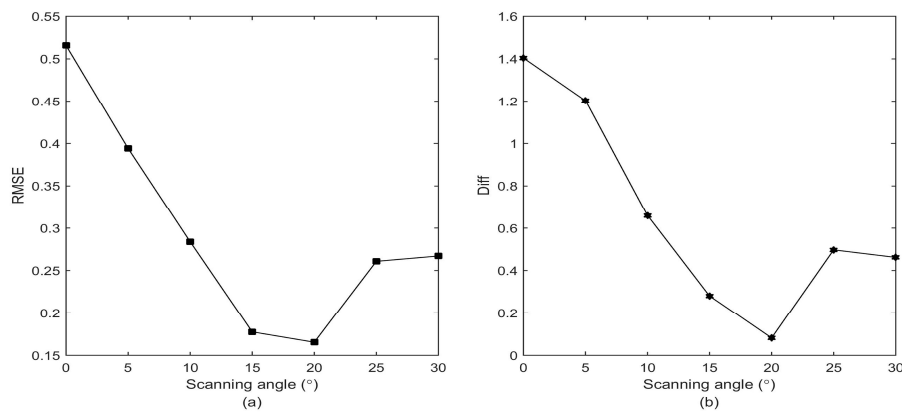


Figure 10. The RMSEs of the foliage profiles (a) and the *Diffs* of the total LAI (b) at scanning angles from 0° to 30° at 5° intervals (the flying altitude and pulse density are 2000 m and four pulses/m², respectively).

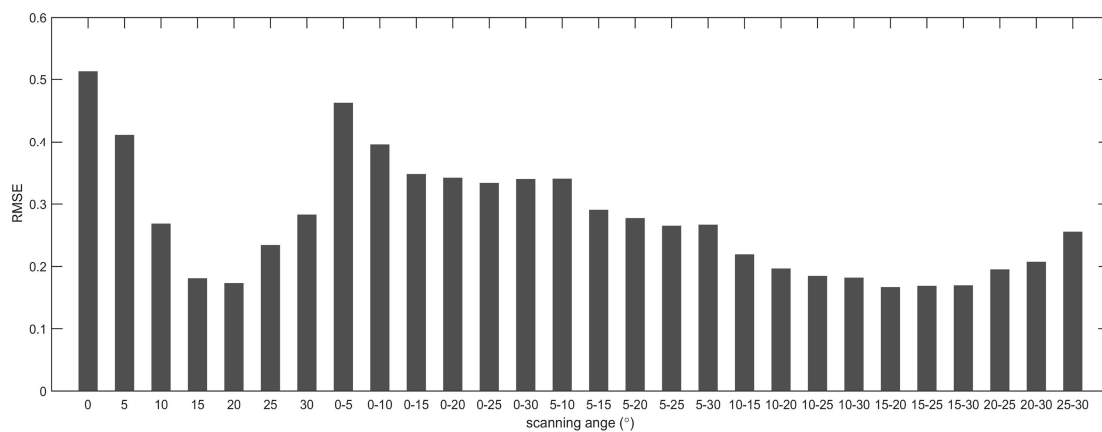


Figure 11. The RMSEs of all single scanning angles and all scanning angle combinations.

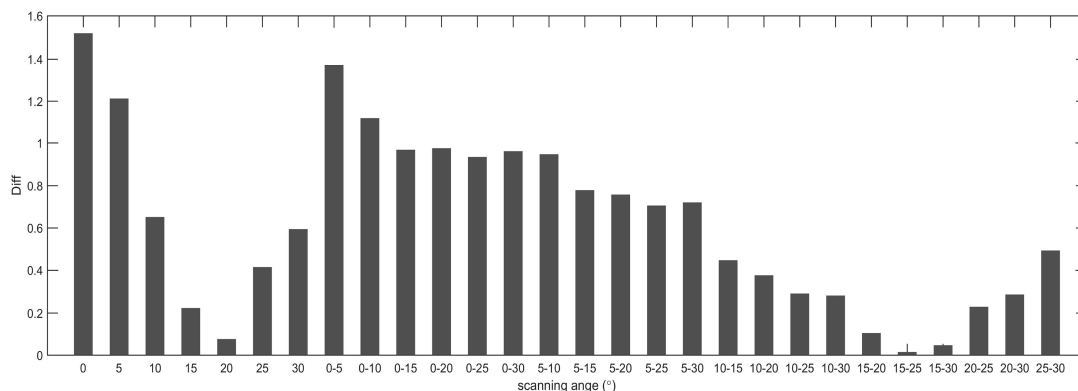


Figure 12. The *Diffs* of all single scanning angles and all scanning angle combinations.

4.3. Effect of Flying Altitude on Foliage Profile Estimation

We estimated the foliage profiles from the simulated full-waveform LiDAR data at flying altitudes from 1000 m to 4000 m at 1000 m intervals to explore the effect of flying altitude on the foliage profile

estimation, and the results are shown in Figure 13. Figure 13a shows the estimated foliage profiles at all flying altitudes, and Figure 13b–e show the histograms of the foliage profiles estimated at each flying altitude. Figure 8 indicates that there was little difference between the foliage profiles derived from the LiDAR data at different flying altitudes. There was no obvious regularity, and the foliage profiles derived from different flying altitudes were all similar.

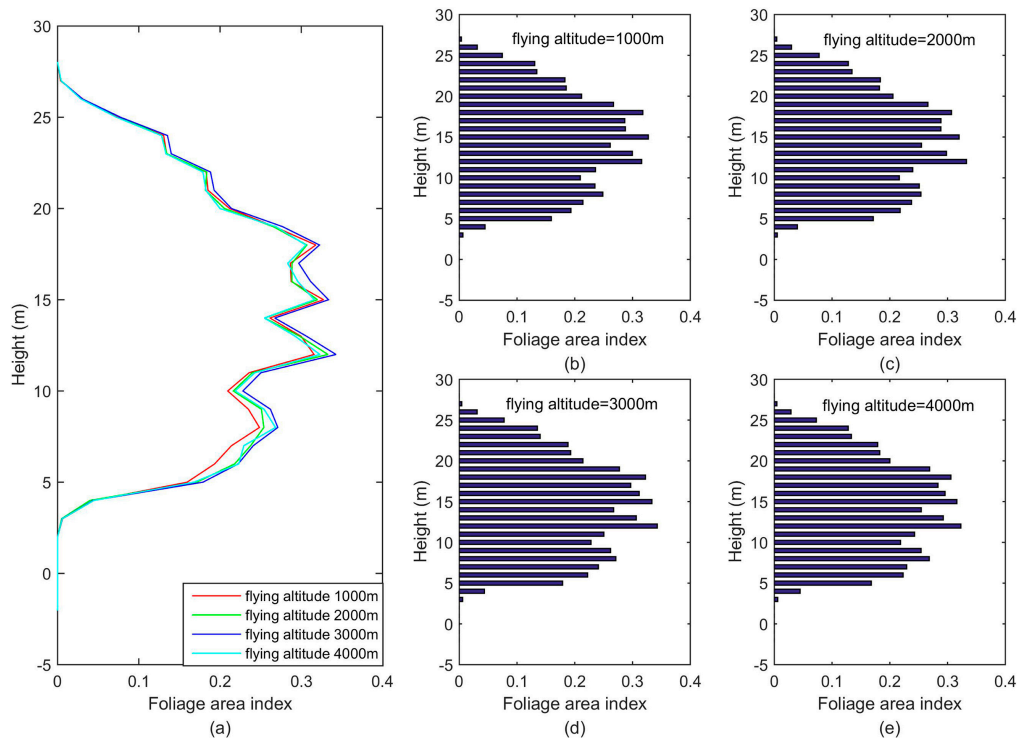


Figure 13. The estimated foliage profiles at flying altitudes from 1000 m to 4000 m at 1000 m intervals (the scanning angle and pulse density are 20° and one pulse/m², respectively). (a) The estimated foliage profiles at all flying altitudes; (b–e) the histograms of the estimated foliage profiles at the flying altitudes of 1000 m, 2000 m, 3000 m, and 4000 m, respectively.

The *RMSEs* of the foliage profiles and the *Diffs* of the total *LAI*s at all flying altitudes were calculated to quantitatively analyse the foliage profile retrieval results, and the results are shown in Figure 14. Figure 14a shows that the *RMSEs* at all flying altitudes were similar, and they were all very small and between 0.16 and 0.19. Although the rate of change of the *RMSE* was small, there was a rising trend when the flying altitude increased from 1000 m to 3000 m and a declining trend when the flying altitude increased from 3000 m to 4000 m. The *RMSE* at the flying altitude of 3000 m was the largest, and it was the smallest at the flying altitude of 1000 m. The *Diff* increased when the flying altitude increased from 1000 m to 3000 m, and it decreased when the flying altitude increased from 3000 m to 4000 m. Therefore, the *Diff* at the flying altitude of 3000 m was the largest, and it was the smallest at the flying altitude of 1000. However, the overall change of the *Diff* was small and was only from 0 to 0.3. Therefore, when the flying altitude increased from 1000 m to 4000 m, the estimation accuracy was highest at the flying altitude of 1000 m and smallest at the flying altitude of 3000 m. However, the *RMSEs* and the *Diffs* at all flying altitudes were very close.

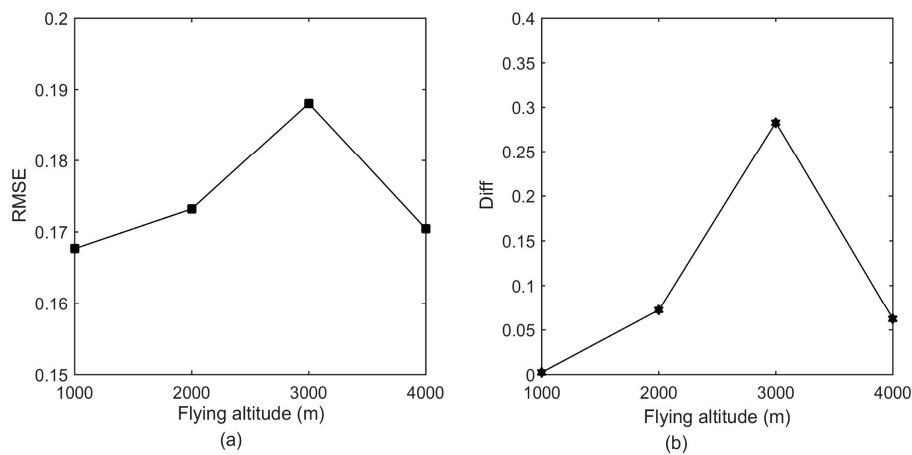


Figure 14. The RMSEs of the foliage profiles (a) and the Diffs of the total LAIs (b) at flying altitudes from 1000 m to 4000 m at 1000 m intervals (the scanning angle and pulse density are 20° and one pulse/m², respectively).

4.4. Effect of LiDAR Pulse Density on Foliage Profile Estimation

The forest foliage profiles were estimated from the airborne small-footprint full-waveform LiDAR data at different pulse densities from 0.25 pulse/m² to eight pulses/m² to explore the influence of pulse density on the forest foliage profile, and the results are shown in Figure 15. Figure 15a shows the estimated foliage profiles at all pulse densities, and Figure 15b–g show the histograms of the estimated foliage profiles at the pulse densities of 0.25 pulse/m², 0.5 pulse/m², one pulse/m², 2 pulses/m², four pulses/m², and eight pulses/m². Figure 15 shows that when the pulse density increased from 0.25 pulse/m² to eight pulses/m², the retrieved foliage profiles were all very close to each other, and there was no obvious change rule. Therefore, when the pulse density increased from 0.25 pulse/m² to eight pulses/m², the effect of pulse density on the foliage profile at plot level was weak.

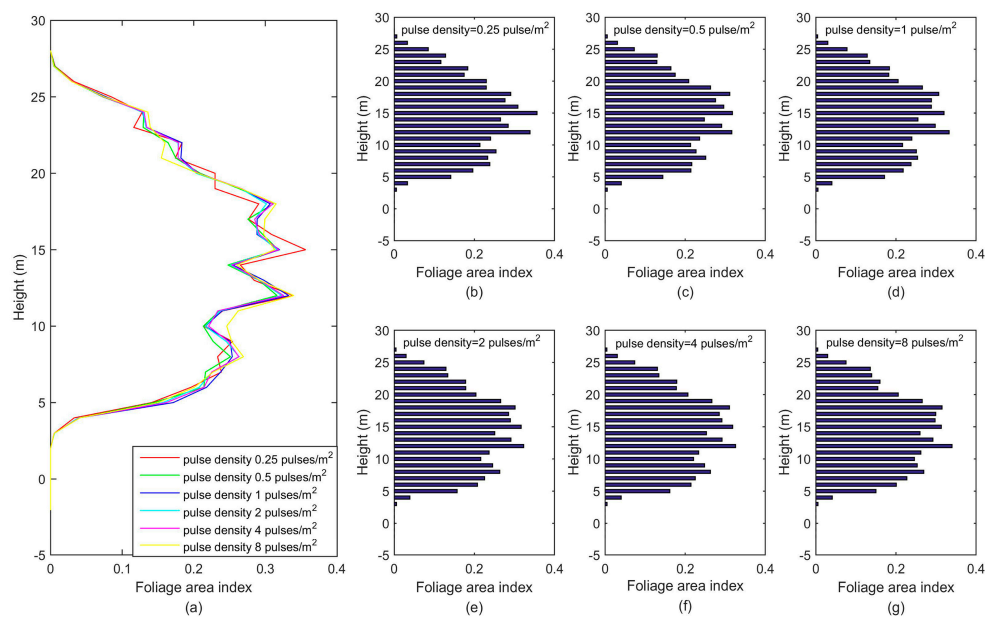


Figure 15. The estimated foliage profiles at pulse densities from 0.25 pulse/m² to eight pulses/m² (the scanning angle and flying altitude are 20° and 2000 m, respectively). (a) the estimated foliage profiles at all pulse densities; (b–g) the histograms of the estimated foliage profiles at pulse densities of 0.25 pulse/m², 0.5 pulse/m², one pulse/m², two pulses/m², four pulses/m², and eight pulses/m².

The RMSEs of the foliage profiles and the *Diffs* of the total LAIs at all pulse densities were calculated to quantitatively analyse the foliage profile retrieval results, and the results are shown in Figure 16. Figure 16a shows that when the pulse density was between 0.25 pulse/m² and eight pulses/m², the RMSEs were all similar, and they were all very small and between 0.16 and 0.18. Figure 16b shows that the *Diff* changed slightly when the pulse densities were between 0.25 pulse/m² and eight pulses/m², and they were all small and within the range of 0.01 to 0.09. Therefore, when the pulse density increased from 0.25 pulse/m² to eight pulses/m², the estimation accuracies of the foliage profiles were similar and remained high.

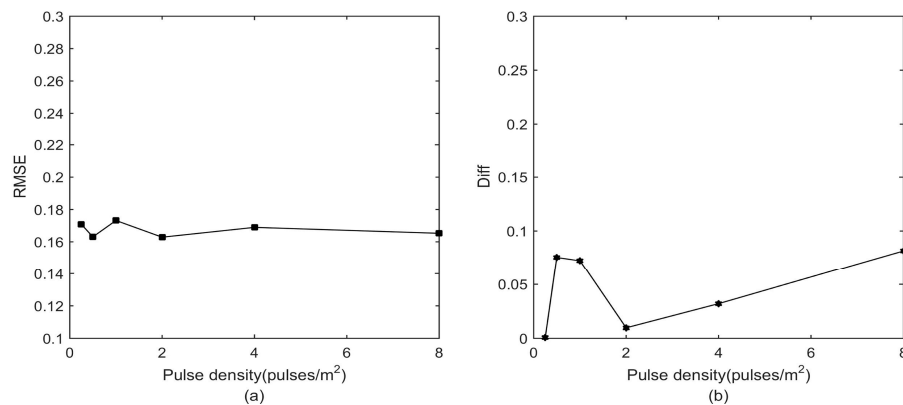


Figure 16. The RMSEs of the foliage profiles (a) and the *Diffs* of the total LAI (b) at pulse densities from 0.25 pulse/m² to eight pulses/m² (the scanning angle and flying altitude are 20° and 2000 m, respectively).

5. Discussion

Tang et al. [24] estimated the vertical LAI distributions from the Laser Vegetation Imaging Sensor (LVIS) large-footprint waveforms based on the GORT model. Our study indicated that the forest foliage profile could be accurately estimated using the GORT model and simulated airborne small-footprint full-waveform LiDAR data. Therefore, the physics-based method used in this study is an efficient foliage profile retrieval method to use when waveform LiDAR data are available. To improve the foliage profile estimation accuracy and minimize the data acquisition costs, the effects of data acquisition conditions on the forest foliage profile estimation were explored, including the scanning angle, flying altitude, and pulse density.

Previous studies have found that when the scanning angle increased, the amount of echo from the ground decreased [28,30,40]. Similarly, the analysis of the influence of the scanning angle on the foliage profile estimation in this study found that when the scanning angle increased, airborne LiDAR acquired a similar return energy from the upper canopy, more return energy from the lower canopy, and less ground return energy. Therefore, when the scanning angle was larger, the foliage area index derived from the GORT model was slightly smaller at the upper canopy and larger at the lower canopy. This result occurs because when using a large scanning angle, the path length through the canopy is longer than in near nadir measurements with a small scanning angle [29]. Thus, more emitted pulses were intercepted by the lower canopy, and fewer echoes backscattered from the ground were detected.

Holmgren et al. [30] simulated the influence of the LiDAR scanning angle on the estimation of canopy height and closure related metrics. The results indicated that these metrics changed quickly when the scanning angle increased from 0° to 20°, and they changed slightly when the scanning angle increased from 20° to 30°. Keränen et al. [29] studied the effect of the scanning angle on the accuracy of an ALS-based forest inventory, and they found that a narrower scanning angle (30°) led to more accurate results than a wider scanning angle (40°). Similarly, the accuracy assessments in this study found that the estimated foliage profile at the scanning angle of 20° was nearest to the simulated foliage profile, and the estimated total LAI at the scanning angle of 20° was the most accurate. Therefore,

the optimal scanning angle for the forest foliage profile estimation was 20° . The sensitivity analyses found that the optimal scanning angle for foliage profile retrieval at plot level is independent of the flying altitude and pulse density when the flying altitude increased from 1000 m to 4000 m and the pulse density increased from 0.25 pulse/m² to four pulses/m². In addition, a combination of multiple scanning angles can improve the foliage profile estimation accuracy, such as the combinations of 15° and 25° and 15° and 30° scanning angles. Of course, more accurate foliage profile estimation methods for combining multiple scanning angles should be explored in future research.

Increasing the flying altitude can enlarge the observation area while retaining the same flying time, thereby decreasing the cost of data acquisition [41]. When the flying altitude was increased, the footprint size was enlarged and the pulse density was decreased, so the return energy was affected. Næsset et al. [42] found that the flying altitude had no effect on the estimation of mean height and volume. A study by Goodwin et al. [43] also reached similar conclusions. In this study, the analysis of the impact of the flying altitude found that the foliage profiles derived from different flying altitudes showed little difference, and they were all close to each other. The error analyses also found that the flying altitude affected the foliage profile and total *LAI* estimation very little, and the effects could be ignored. This phenomenon might be due to the opposite effects for the return energy profile derived from the increase of the footprint size and the decrease of the pulse density. Therefore, the flying altitude can affect the return energy, but the prediction error of the foliage profile and the total *LAI* do not change much. This result is in agreement with the findings of Næsset et al. [44]

Several studies have explored the influence of pulse density on forest parameter estimations [45–47]. These studies found that the precision of the canopy height, diameter at breast height, and stand volume estimations were all insensitive to the reduction in pulse density until the pulse density dropped below one pulse/m² [45,46]. When the pulse density was smaller, the return energy of the whole plot was smaller. Therefore, the pulse density could significantly affect the return energy profile of the plot. In this study, the analysis of the sensitivity of the foliage profile estimation to pulse density found that the foliage profiles derived from the different pulse densities were all close to each other, and the *RMSEs* and *Diff*s were all very small. Therefore, the effect of pulse density on foliage profile retrieval was weak and could be ignored. Of course, the pulse densities used in this study were only from 0.25 pulse/m² to eight pulses/m², which might not be sufficient to draw these conclusions. A larger range of pulse densities and other forest types need to be studied in further research. Although the return energy profiles with different pulse densities were obviously different, the foliage profile was essentially constant. This was because the foliage profile was derived from the GORT model, which was based on the gap probability.

6. Conclusions

We explored the effects of the airborne LiDAR scanning angle, flying altitude, and pulse density on forest foliage profile retrieval for the first time, to our knowledge. The results indicated that the scanning angle is an important influence factor in foliage profile retrieval, and the optimal scanning angle for foliage profile estimations is 20° . The optimal scanning angle was independent of the flying altitude and pulse density. In addition, scanning angle combinations of 15° and 25° and 15° and 30° can improve the foliage profile estimation accuracy. A more accurate method that combines multiple scanning angles for foliage profile estimations should be studied in future research. The effects of flying altitude and pulse density on foliage profile retrieval were small with no obvious regularity, so they could all be ignored.

In general, the forest foliage profile estimation was significantly affected by the airborne LiDAR scanning angle, and the effects of flying altitude and pulse density on the foliage profile estimation were small and could be ignored. These sensitivity analyses were very important for selecting optimal instrument operational parameters to acquire more accurate foliage profiles and minimize data acquisition costs. Overall, our results provide reliable and useful information for the forest and ecological researchers using LiDAR data.

Acknowledgments: This work was supported by the National Key R&D Program of China (No. 2017YFA0603002) and National Natural Science Foundation of China (Nos. 41371350, 41671434, and 41431179). We received funds for covering the costs to publish in open access.

Author Contributions: Haiming Qin designed the study, collected and analyzed the data, and wrote the manuscript. Cheng Wang designed the study, and wrote the manuscript. Xiaohuan Xi searched the literature, analyzed the data, and revised the manuscript. Jianlin Tian analyzed the data and revised the manuscript. Guoqing Zhou collected the data and revised the manuscript. The manuscript was improved by the contributions of all of the co-authors.

Conflicts of Interest: The authors declare no conflict of interest.

References

- Lang, A.R.G.; McMurtrie, R.E.; Benson, M.L. Validity of surface area indices of pinus radiata estimated from transmittance of the sun's beam. *Agric. For. Meteorol.* **1991**, *57*, 157–170. [[CrossRef](#)]
- Gower, S.T.; Norman, J.M. Rapid estimation of leaf area index in conifer and broad-leaf plantations. *Ecology* **1991**, *72*, 1896–1900. [[CrossRef](#)]
- Ellsworth, D.S.; Reich, P.B. Canopy structure and vertical patterns of photosynthesis and related leaf traits in a deciduous forest. *Oecologia* **1993**, *96*, 169–178. [[CrossRef](#)] [[PubMed](#)]
- Parker, G.G.; Lefsky, M.A.; Harding, D.J. Light transmittance in forest canopies determined using airborne laser altimetry and in-canopy quantum measurements. *Remote Sens. Environ.* **2001**, *76*, 298–309. [[CrossRef](#)]
- Drake, J.B.; Dubayah, R.O.; Knox, R.G.; Clark, D.B.; Blair, J.B. Sensitivity of large-footprint lidar to canopy structure and biomass in a neotropical rainforest. *Remote Sens. Environ.* **2002**, *81*, 378–392. [[CrossRef](#)]
- Stark, S.C.; Leitold, V.; Wu, J.L.; Hunter, M.O.; de Castilho, C.V.; Costa, F.R.C.; McMahon, S.M.; Parker, G.G.; Shimabukuro, M.T.; Lefsky, M.A.; et al. Amazon forest carbon dynamics predicted by profiles of canopy leaf area and light environment. *Ecol. Lett.* **2012**, *15*, 1406–1414. [[CrossRef](#)] [[PubMed](#)]
- Toda, M.; Yokozawa, M.; Sumida, A.; Watanabe, T.; Hara, T. Foliage profiles of individual trees determine competition, self-thinning, biomass and npp of a ctyptomeria japonica forest stand: A simulation study based on a stand-scale process-based forest model. *Ecol. Model.* **2009**, *220*, 2272–2280. [[CrossRef](#)]
- Swatantran, A.; Dubayah, R.; Roberts, D.; Hofton, M.; Blair, J.B. Mapping biomass and stress in the sierra nevada using lidar and hyperspectral data fusion. *Remote Sens. Environ.* **2011**, *115*, 2917–2930. [[CrossRef](#)]
- Wilson, J.W. Inclined point quadrats. *New Phytol.* **1960**, *59*, 1–7. [[CrossRef](#)]
- Wilson, J. Estimation of foliage denseness and foliage angle by inclined point quadrats. *Aust. J. Bot.* **1963**, *11*, 95–105. [[CrossRef](#)]
- Cohen, W.B.; Maersperger, T.K.; Gower, S.T.; Turner, D.P. An improved strategy for regression of biophysical variables and landsat etm+ data. *Remote Sens. Environ.* **2003**, *84*, 561–571. [[CrossRef](#)]
- Morisette, J.T.; Baret, F.; Privette, J.L.; Myneni, R.B.; Nickeson, J.E.; Garrigues, S.; Shabanov, N.V.; Weiss, M.; Fernandes, R.; Leblanc, S.G. Validation of global moderate-resolution lai products: A framework proposed within the ceos land product validation subgroup. *IEEE Trans. Geosci. Remote Sens.* **2006**, *44*, 1804. [[CrossRef](#)]
- Zhang, Y.Q.; Chen, J.M.; Miller, J.R.; Noland, T.L. Leaf chlorophyll content retrieval from airborne hyperspectral remote sensing imagery. *Remote Sens. Environ.* **2008**, *112*, 3234–3247. [[CrossRef](#)]
- Yang, X.; Yu, Y.; Fan, W. Chlorophyll content retrieval from hyperspectral remote sensing imagery. *Environ. Monit. Assess.* **2015**, *187*, 1–13. [[CrossRef](#)] [[PubMed](#)]
- Harding, D.J.; Lefsky, M.A.; Parker, G.G.; Blair, J.B. Laser altitude canopy height profiles methods and validation for closed-canopy, broadleaf forests. *Remote Sens. Environ.* **2001**. [[CrossRef](#)]
- Fieber, K.D.; Davenport, I.J.; Tanase, M.A.; Ferryman, J.M.; Gurney, R.J.; Walker, J.P.; Hacker, J.M. Preliminary leaf area index estimates from airborne small footprint full-waveform lidar data. In Proceedings of the 2013 IEEE International Geoscience and Remote Sensing Symposium-IGARSS, Melbourne, Australia, 21–26 July 2013; pp. 3379–3382.
- Su, Y.; Guo, Q.; Xue, B.; Hu, T.; Alvarez, O.; Tao, S.; Fang, J. Spatial distribution of forest aboveground biomass in china: Estimation through combination of spaceborne lidar, optical imagery, and forest inventory data. *Remote Sens. Environ.* **2016**, *173*, 187–199. [[CrossRef](#)]
- Wang, C.; Glenn, N.F. A linear regression method for tree canopy height estimation using airborne lidar data. *Can. J. Remote Sens.* **2008**, *34*, S217–S227. [[CrossRef](#)]

19. Korhonen, L.; Korpela, I.; Heiskanen, J.; Maltamo, M. Airborne discrete-return lidar data in the estimation of vertical canopy cover, angular canopy closure and leaf area index. *Remote Sens. Environ.* **2011**, *115*, 1065–1080. [[CrossRef](#)]
20. Alonzo, M.; Bookhagen, B.; McFadden, J.P.; Sun, A.; Roberts, D.A. Mapping urban forest leaf area index with airborne lidar using penetration metrics and allometry. *Remote Sens. Environ.* **2015**, *162*, 141–153. [[CrossRef](#)]
21. Rejou-Mechain, M.; Tymen, B.; Blanc, L.; Fauset, S.; Feldpausch, T.R.; Monteagudo, A.; Phillips, O.L.; Richard, H.; Chave, J. Using repeated small-footprint lidar acquisitions to infer spatial and temporal variations of a high-biomass neotropical forest. *Remote Sens. Environ.* **2015**, *169*, 93–101. [[CrossRef](#)]
22. Jupp, D.L.; Culvenor, D.S.; Lovell, J.L.; Newnham, G.J.; Strahler, A.H.; Woodcock, C.E. Estimating forest lai profiles and structural parameters using a ground-based laser called ‘echidna’. *Tree Physiol.* **2009**, *29*, 171–181. [[CrossRef](#)] [[PubMed](#)]
23. Fieber, K.D.; Davenport, I.J.; Tanase, M.A.; Ferryman, J.M.; Gurney, R.J.; Walker, J.P.; Hacker, J.M. Effective lai and chp of a single tree from small-footprint full-waveform lidar. *IEEE Geosci. Remote Sens.* **2014**, *11*, 1634–1638. [[CrossRef](#)]
24. Tang, H.; Dubayah, R.; Swatantran, A.; Hofton, M.; Sheldon, S.; Clark, D.B.; Blair, B. Retrieval of vertical lai profiles over tropical rain forests using waveform lidar at la selva, costa rica. *Remote Sens. Environ.* **2012**, *124*, 242–250. [[CrossRef](#)]
25. Ma, H.; Song, J.; Wang, J. Forest canopy lai and vertical favd profile inversion from airborne full-waveform lidar data based on a radiative transfer model. *Remote Sens.* **2015**, *7*, 1897–1914. [[CrossRef](#)]
26. Zhao, F.; Yang, X.Y.; Strahler, A.H.; Schaaf, C.L.; Yao, T.; Wang, Z.S.; Roman, M.O.; Woodcock, C.E.; Ni-Meister, W.; Jupp, D.L.B.; et al. A comparison of foliage profiles in the sierra national forest obtained with a full-waveform under-canopy evi lidar system with the foliage profiles obtained with an airborne full-waveform lvis lidar system. *Remote Sens. Environ.* **2013**, *136*, 330–341. [[CrossRef](#)]
27. Morsdorf, F.; Frey, O.; Meier, E.; Itten, K.I.; Allgoewer, B. Assessment of the influence of flying altitude and scan angle on biophysical vegetation products derived from airborne laser scanning. *Int. J. Remote Sens.* **2008**, *29*, 1387–1406. [[CrossRef](#)]
28. Lovell, J.L.; Jupp, D.L.B.; Newnham, G.J.; Coops, N.C.; Culvenor, D.S. Simulation study for finding optimal lidar acquisition parameters for forest height retrieval. *For. Ecol. Manag.* **2005**, *214*, 398–412. [[CrossRef](#)]
29. Keränen, J.; Maltamo, M.; Packalen, P. Effect of flying altitude, scanning angle and scanning mode on the accuracy of als based forest inventory. *Int. J. Appl. Earth Obs.* **2016**, *52*, 349–360. [[CrossRef](#)]
30. Holmgren, J.; Nilsson, M.; Olsson, H. Simulating the effects of lidar scanning angle for estimation of mean tree height and canopy closure. *Can. J. Remote Sens.* **2003**, *29*, 623–632. [[CrossRef](#)]
31. Kükenbrink, D.; Schneider, F.D.; Leiterer, R.; Schaepman, M.E.; Morsdorf, F. Quantification of hidden canopy volume of airborne laser scanning data using a voxel traversal algorithm. *Remote Sens. Environ.* **2017**, *194*, 424–436. [[CrossRef](#)]
32. Fettig, C.J.; Allen, K.K.; Borys, R.R.; Christopherson, J.; Dabney, C.P.; Eager, T.J.; Gibson, K.E.; Hebertson, E.G.; Long, D.F.; Munson, A.S.; et al. Effectiveness of bifenthrin (onyx) and carbaryl (sevin sl) for protecting individual, high-value conifers from bark beetle attack (Coleoptera: Curculionidae: Scolytinae) in the western united states. *J. Econ. Entomol.* **2006**, *99*, 1691–1698. [[CrossRef](#)] [[PubMed](#)]
33. Gastellu-Etchegorry, J.-P.; Yin, T.; Lauret, N.; Cajgfinger, T.; Gregoire, T.; Grau, E.; Feret, J.-B.; Lopes, M.; Guilleux, J.; Dedieu, G.; et al. Discrete anisotropic radiative transfer (dart 5) for modeling airborne and satellite spectroradiometer and lidar acquisitions of natural and urban landscapes. *Remote Sens.* **2015**, *7*, 1667–1701. [[CrossRef](#)]
34. Yin, T.; Gastellu-Etchegorry, J.P.; Grau, E.; Lauret, N.; Rubio, J. Simulating satellite waveform lidar with dart model. In Proceedings of the 2013 IEEE International Geoscience and Remote Sensing Symposium-IGARSS, Melbourne, Australia, 21–26 July 2013.
35. Yin, T.; Lauret, N.; Gastellu-Etchegorry, J.-P. Simulation of satellite, airborne and terrestrial lidar with dart (ii): Als and tls multi-pulse acquisitions, photon counting, and solar noise. *Remote Sens. Environ.* **2016**, *184*, 454–468. [[CrossRef](#)]
36. Gastellu-Etchegorry, J.-P.; Yin, T.; Lauret, N.; Grau, E.; Rubio, J.; Cook, B.D.; Morton, D.C.; Sun, G. Simulation of satellite, airborne and terrestrial lidar with dart (i): Waveform simulation with quasi-monte carlo ray tracing. *Remote Sens. Environ.* **2016**, *184*, 418–435. [[CrossRef](#)]

37. Fieber, K.D.; Davenport, I.J.; Tanase, M.A.; Ferryman, J.M.; Gurney, R.J.; Becerra, V.M.; Walker, J.P.; Hacker, J.M. Validation of canopy height profile methodology for small-footprint full-waveform airborne lidar data in a discontinuous canopy environment. *ISPRS J. Photogramm.* **2015**, *104*, 144–157. [[CrossRef](#)]
38. Nie, S.; Wang, C.; Dong, P.; Xi, X. Estimating leaf area index of maize using airborne full-waveform lidar data. *Remote Sens. Lett.* **2016**, *7*, 111–120. [[CrossRef](#)]
39. Chen, J.M.; Menges, C.H.; Leblanc, S.G. Global mapping of foliage clumping index using multi-angular satellite data. *Remote Sens. Environ.* **2005**, *97*, 447–457. [[CrossRef](#)]
40. Disney, M.I.; Kalogirou, V.; Lewis, P.; Prieto-Blanco, A.; Hancock, S.; Pfeifer, M. Simulating the impact of discrete-return lidar system and survey characteristics over young conifer and broadleaf forests. *Remote Sens. Environ.* **2010**, *114*, 1546–1560. [[CrossRef](#)]
41. Næsset, E. Area-based inventory in norway—From innovation to an operational reality. In *Forestry Applications of Airborne Laser Scanning: Concepts and Case Studies*; Maltamo, M., Næsset, E., Vauhkonen, J., Eds.; Springer: Dordrecht, The Netherlands, 2014; pp. 215–240.
42. Nasset, E. Effects of different flying altitudes on biophysical stand properties estimated from canopy height and density measured with a small-footprint airborne scanning laser. *Remote Sens. Environ.* **2004**, *91*, 243–255. [[CrossRef](#)]
43. Goodwin, N.R.; Coops, N.C.; Culvenor, D.S. Assessment of forest structure with airborne lidar and the effects of platform altitude. *Remote Sens. Environ.* **2006**, *103*, 140–152. [[CrossRef](#)]
44. Næsset, E. Effects of different sensors, flying altitudes, and pulse repetition frequencies on forest canopy metrics and biophysical stand properties derived from small-footprint airborne laser data. *Remote Sens. Environ.* **2009**, *113*, 148–159. [[CrossRef](#)]
45. Jakubowski, M.K.; Guo, Q.; Kelly, M. Tradeoffs between lidar pulse density and forest measurement accuracy. *Remote Sens. Environ.* **2013**, *130*, 245–253. [[CrossRef](#)]
46. Michael, S.W.; Thomas, A.; Susana, G.A.; Hamish, M.; Pete, W. The influence of lidar pulse density and plot size on the accuracy of new zealand plantation stand volume equations. *N. Z. J. For. Sci.* **2013**, *43*. [[CrossRef](#)]
47. Michael, S.W.; Andrew, M.; Pete, W.; Aaron, G. The influence of lidar pulse density on the precision of inventory metrics in young unthinned douglas-fir stands during initial and subsequent lidar acquisitions. *N. Z. J. For. Sci.* **2014**, *44*. [[CrossRef](#)]



© 2017 by the authors. Licensee MDPI, Basel, Switzerland. This article is an open access article distributed under the terms and conditions of the Creative Commons Attribution (CC BY) license (<http://creativecommons.org/licenses/by/4.0/>).